Characterizations of tropospheric turbulence and stability layers from aircraft observations

Citation: Cho, John Y. N. et al. "Characterizations of Tropospheric Turbulence and Stability Layers from Aircraft Observations." Journal of Geophysical Research 108, D20 (October 2003): 5

As Published: http://dx.doi.org/10.1029/2002JD002820

Publisher: American Geophysical Union (AGU)

Persistent URL: http://hdl.handle.net/1721.1/110975

Version: Final published version: final published article, as it appeared in a journal, conference proceedings, or other formally published context

Characterizations of tropospheric turbulence and stability layers from aircraft observations

John Y. N. Cho[1] and Reginald E. Newell

Department of Earth, Atmospheric, and Planetary Sciences, Massachusetts Institute of Technology, Cambridge, Massachusetts, USA

Bruce E. Anderson, John D. W. Barrick, and K. Lee Thornhill

NASA Langley Research Center, Hampton, Virginia, USA

Received 2 August 2002; revised 12 December 2002; accepted 23 December 2002; published 26 August 2003.

[1] Velocity, temperature, and specific humidity data collected by aircraft at 20-Hz resolution are analyzed for stability and turbulence parameters. Over 100 vertical profiles (mostly over the ocean) with a total of over 300 km in vertical airspace sampled are used. The compiled statistics show that anisotropy in the velocity fluctuations prevail down to the smallest spatial separations measured. A partitioning of convective versus dynamical instability indicates that in the free troposphere, the ratio of shear-produced turbulence to convectively produced turbulence increases from roughly 2:1 for weak turbulence ($\epsilon < 10^{-4}$ m^2 s^{-3}) to perhaps 3:1 for strong turbulence ($\epsilon > 10^{-4}$ m^2 s^{-3}). For the boundary layer, this ratio is close to 1:1 for weak turbulence and roughly 2:1 for strong turbulence. There is also a correlation between the strength of the vertical shear in horizontal winds and the turbulence intensity. In the free troposphere the turbulence intensity is independent of the degree of static stability, whereas in the boundary layer the turbulence intensity increases with a fall in static stability. Vertical humidity gradients correlate with static stability for strong humidity gradients, which supports the basic notion that stable layers impede vertical mixing of trace gases and aerosols. Vertical shear correlates with vertical humidity gradient, so it appears that the effect of differential advection creating tracer gradients dominates the effect of differential advection destroying tracer gradients through shear-induced turbulence. *INDEX TERMS:* 3307 Meteorology and Atmospheric Dynamics: Boundary layer processes; 3314 Meteorology and Atmospheric Dynamics: Convective processes; 3379 Meteorology and Atmospheric Dynamics: Turbulence; *KEYWORDS:* clear air turbulence, stable layers, tracer mixing, shear instability, convective instability

Citation: Cho, J. Y. N., R. E. Newell, B. E. Anderson, J. D. W. Barrick, and K. L. Thornhill, Characterizations of tropospheric turbulence and stability layers from aircraft observations, *J. Geophys. Res.*, *108*(D20), 8784, doi:10.1029/2002JD002820, 2003.

1. Introduction

[2] Profiles of the Earth's atmosphere show varying degrees of stratification at a wide range of vertical scales. At large scales the stratification, as measured by the mean vertical temperature gradient, is used to define the major divisions of the neutral atmosphere: troposphere, stratosphere, mesosphere, and thermosphere. Zooming in to smaller scales, however, one discovers that embedded in each division are layers in which the sense of the temperature gradient is reversed. For example, the troposphere contains inversion layers through which the temperature increases with altitude, a kind of miniature stratosphere-within-a-troposphere phenomenon. If one goes to even smaller scales, then one observes reverses within the reverses, and so on to the limit of fluctuation dissipation by thermal diffusion.

[3] Layers of static stability have important consequences for trace constituent distribution as can be clearly seen from the capping of the boundary layer. They also exist and play an important role in trace gas and aerosol distribution in the free troposphere [*Swap and Tyson*, 1999; *Cho et al.*, 2001; *Hobbs*, 2002]. At small thicknesses (of order 1 m or less) they are often called temperature sheets [*Dalaudier et al.*, 1994] and are of interest for their effects on radio and optical wave propagation.

[4] Instability and turbulence also exist throughout the atmosphere. If they occur within statically stable regions, they exist as layers that can be as thin as several meters [e.g., *Muschinski and Wode*, 1998]. One school of thought ascribes the formation of temperature sheets to the action of such turbulent layers on the background temperature gradient (the ''sheet and layer model''), with Kelvin-Helmholtz instability (KHI) as the generation mechanism [*Woods*, 1969]. Another theory invokes viscosity waves,

[1]Now at Lincoln Laboratory, Massachusetts Institute of Technology, Lexington, Massachusetts, USA.

0148-0227/03/2002JD002820$09.00

not turbulence, as the creator of temperature sheets [*Hooke and Jones*, 1986; *Hocking et al.*, 1991].

[5] Encounters with three-dimensional (3-D) turbulence are thought to be the rapid, penultimate step in the vertical-scale cascade of atmospheric tracers, with the final step, of course, being molecular diffusion. Because of the very anisotropic horizontal to vertical aspect ratio in the atmosphere, tracer filaments produced by large-scale differential advection are expected to be dissipated by processes acting along the vertical dimension [*Haynes and Anglade*, 1997].

[6] Encounters with 3-D turbulence at a more immediate "gut" level are events that aircraft passengers would like to avoid. Aside from turbulence due to convective storms, clear air turbulence (CAT) is invisible to the pilot and is difficult to forecast. KHI and breaking mountain waves are believed to be the main culprits, and forecasting techniques have been developed for both of these turbulence generators [e.g., *Ellrod and Knapp*, 1992; *Bacmeister et al.*, 1994]. There has been recent evidence, however, of CAT arising from neither of these mechanisms [*Cho et al.*, 1999], and it has also been suggested that differential radiative heating by high-humidity layers might trigger instabilities [*Newell et al.*, 1999].

[7] In this paper we analyze vertical profile data taken by the NASA P-3B aircraft during the Transport and Chemical Evolution Over the Pacific (TRACE-P) campaign. Horizontal and vertical velocity, temperature, and specific humidity effectively sampled at 20 Hz are used to compile statistics on various stability and turbulence parameters. Using these statistics, we examine the following questions: What is the probability distribution of the turbulence energy dissipation rate ϵ? What are the relative contributions of dynamical versus convective instability to turbulence generation? Do high-humidity layers contribute to CAT? How efficiently does 3-D turbulence destroy vertical gradients in tracers? How do the answers to the above questions differ for the boundary layer versus the free troposphere?

2. Experiment Description

[8] TRACE-P, which took place during February–April 2001, was the latest in the line of NASA Global Tropospheric Experiment (GTE) aircraft missions [*McNeal et al.*, 1983] conducted to study atmospheric chemistry. This campaign focused on evaluating the outflow of chemically and radiatively important gases and aerosols from the Asian continent, and, as such, was staged in the western Pacific. For an overview of the mission with flight track maps, instrument lists, etc., see *Jacob et al.* [2003]. A detailed summary of the meteorological conditions is given by *Fuelberg et al.* [2003].

[9] Two aircraft, the NASA-Dryden DC-8 and Wallops P-3B, were used during TRACE-P. This study will utilize data from the P-3B because it was equipped with a turbulent air motion measurement system (TAMMS) capable of determining three-dimensional winds along with fast fluctuations of pressure, temperature, and water vapor at an effective sampling rate of 20 Hz. The TAMMS is composed of (1) a radome instrumented with flush pressure ports coupled with absolute and differential pressure transducers and temperature sensors, (2) aircraft inertial and satellite navigation systems, (3) a central data acquisition/processing system, and (4) trace gas sensors. See *Considine et al.* [1999] for a more detailed description of the TAMMS and *Barrick et al.* [1996] for details of applied calibration procedures.

[10] The turboprop P-3B had a ceiling of 8 km and was mainly used for sampling the boundary layer up to mid-tropospheric heights. The DC-8 with its higher ceiling covered the upper troposphere and lower stratosphere, but it was not equipped with a turbulence measurement system. Typical flight patterns for the P-3B consisted of level segments at different altitudes connected by steep ascents and descents. Since we are interested in vertical gradient quantities, we will extract profile data provided by these up- and down-legs.

3. Data Analysis Issues

[11] The TAMMS took data during flights 4 through 24. The primary inertial navigation system (used to calculate the wind components), however, was turned off during flights 4, 11, and 24, so we did not include data from those flights. The Lyman-α hygrometer was not operating properly during flights 19 and 21, so we also omitted those flights. In the remaining 16 flights, there were 184 profiles of vertical extent longer than 1000 m. We carefully went through each of these profiles and looked at the velocity, temperature, and specific humidity data. If there was a data gap or abrupt discontinuity in any of those measured parameters, we eliminated that profile from consideration. Being quite conservative in the quality control step, we were left with 122 profile segments for a total of 333 km of vertically sampled airspace.

[12] In this paper we use the term "boundary layer" rather loosely. There seems to be no universally accepted precise definition of where the planetary (or atmospheric) boundary layer ends. We elected to use the base of the capping inversion as indicated by the virtual potential temperature profile. We could have also used tracer profiles to mark the altitude where constant mixing ratios ended. However, these heights were not always coincident for different tracers, and, therefore, it was difficult to decide which height should be used for the top of the boundary layer. A consequence of using the base of the capping inversion to delineate the boundary layer is that a regime that some call the buffer layer [*Russell et al.*, 1998] may be included in our definition of the boundary layer. A buffer layer is observed to be intermittently turbulent and not necessarily well mixed, so these characteristics could be mixed into our boundary layer data.

[13] We did not attempt to parse the results according to the prevailing synoptic conditions such as high versus low pressure systems. Collection of data spread out over more varied conditions could lead to further studies along these lines that may shed light on the dependence of turbulence outbreak on larger scale phenomena.

[14] When we write "vertical profile," it is, of course, not literally correct for fixed-wing aircraft data. For the P-3B, which typically flies at $\sim$150 m s^{-1} and ascends/descends at $\sim$5 m s^{-1}, the slope is about 30:1. However,

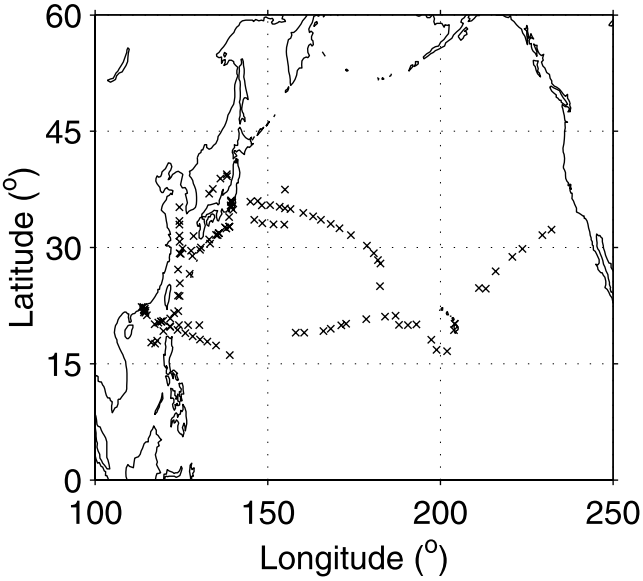

Figure 1. Locations of the vertical profiles used in this paper marked by crosses.

the aspect ratio of the large-scale atmosphere is much larger, roughly suggested by the inverse of Prandtl's ratio f/N, where f is the Coriolis parameter and N is the Brunt-Väisälä frequency [e.g., *Charney*, 1971]. For the midlatitude troposphere this ratio is about 120:1. Inside convective storms and regions of 3-D turbulence, this scaling does not hold. For scales inside or smaller than the inertial range of turbulence, fluctuating quantities tend toward isotropy, although there is ongoing debate about how isotropic turbulence can be inside a real stratified shear flow even at these small scales [e.g., *Smyth and Moum*, 2000]. The outer scale of turbulence depends on ϵ and N [*Weinstock*, 1978], but a reasonable free tropospheric value seems to be $\sim$100 m [e.g., *Cho et al.*, 1999]. The "vertical profile" approximation should hold for Δz quantities greater than the turbulence outer scale, where Δz is the difference in altitude of two points.

[15] To characterize turbulence intensity, we chose the mean turbulent energy dissipation rate ϵ, since it is commonly used in both theoretical and experimental turbulence literature. Physically, ϵ represents the rate of energy dissipated by viscosity after the energy has cascaded down from large to small scales through nonlinear flow interactions characteristic of turbulence. In this sense, ϵ is also the mean kinetic energy flux through the turbulent cascade and is independent of scale.

[16] To calculate ϵ, we followed the procedure adopted by *Meischner et al.* [2001]. The second-order structure functions for u, v, and w (the zonal, meridional, and vertical velocity components) were computed directly from the 20-Hz time series. In the time domain, the second-order structure function for zonal velocity is given by

$$D_{uu}(\Delta t) = \left\langle [u(t+\Delta t) - u(t)]^2 \right\rangle \tag{1}$$

where Δt is the chosen time increment over which to take the difference. For the meridional and vertical components, replace us by v or w. For sufficiently small Δt, the aircraft travels in a straight line, so the structure functions can be easily transformed from the temporal to the spatial domain using the airspeed U_a by letting $\Delta t = r/U_a$, where r is the spatial separation between the differenced points.

[17] For locally isotropic turbulence, ϵ can be calculated from $D_{TT} = 4C(\epsilon r)^{2/3}/3$ [*Monin and Yaglom*, 1975], where D_{TT} is the transverse (velocity component normal to the flight direction) structure function and C is a constant. We will use $C = 2.05$ [*Panofsky and Dutton*, 1984; *Paluch and Baumgartner*, 1989]. For purely horizontal flights, which is not a bad assumption considering our gradual ascent/descent slopes, $D_{TT} = D_{ww}$, so it is possible to estimate ϵ from w only. However, we can also include the other components, since there is a horizontal transverse direction, which may improve the statistical accuracy. Since $D_{uu} + D_{vv} = 7D_{TT}/4$ for isotropic turbulence, an equal weighting of the three orthogonal components yields [*Meischner et al.*, 2001]

$$D_{TT} = \frac{1}{3}\left[\frac{8}{7}(D_{uu} + D_{vv}) + D_{ww}\right]. \tag{2}$$

[18] We also computed a ratio $I = (7/4)[D_{ww}/(D_{uu} + D_{vv})]$, which should be unity for isotropy. If $I < 1$, then there is more energy in the horizontal motions than in the vertical motions (the expected case for large-scale flow). This ratio, then, should increase from a small fraction toward 1 as the r used in the calculation decreases into inertial subrange scales.

[19] To calculate the vertical gradient quantities, we first interpolated the data onto a uniform 1-m altitude spacing. Then we simply took the difference in the quantity divided by a chosen Δz. We calculated the square of the vertical shear in horizontal winds, $(dU/dz)^2 = [(u(z + \Delta z) - u(z))^2 + (v(z + \Delta z) - v(z))^2]/(\Delta z)^2$; the vertical gradient

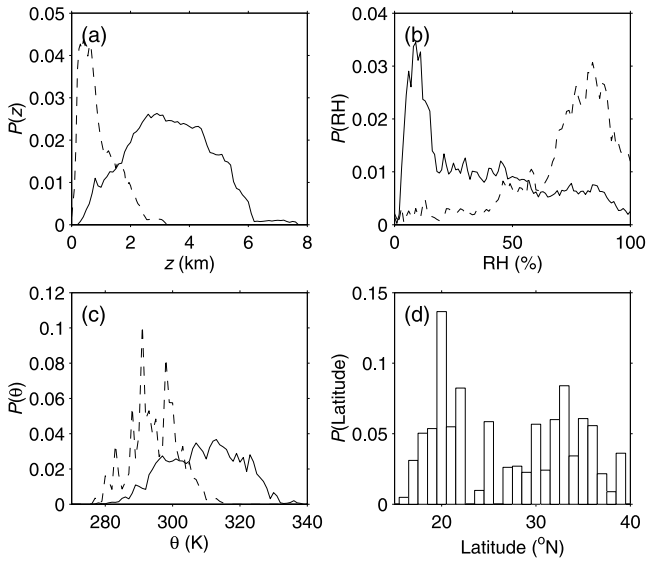

Figure 2. Probability distribution functions of the number of data points with respect to (a) altitude, (b) relative humidity, (c) potential temperature, and (d) latitude. For (a) through (c) the solid line represents the free troposphere and the dashed line denotes the boundary layer.

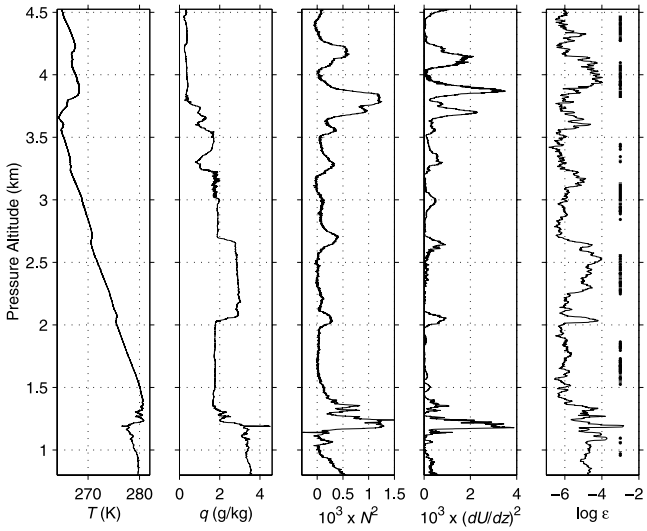

Figure 3. Vertical profile taken at 30°N, 131°E, on March 31, 2001, around 0430 UT. The vertical lines at log $\epsilon = -3$ indicate heights where $Ri \leq 1/4$.

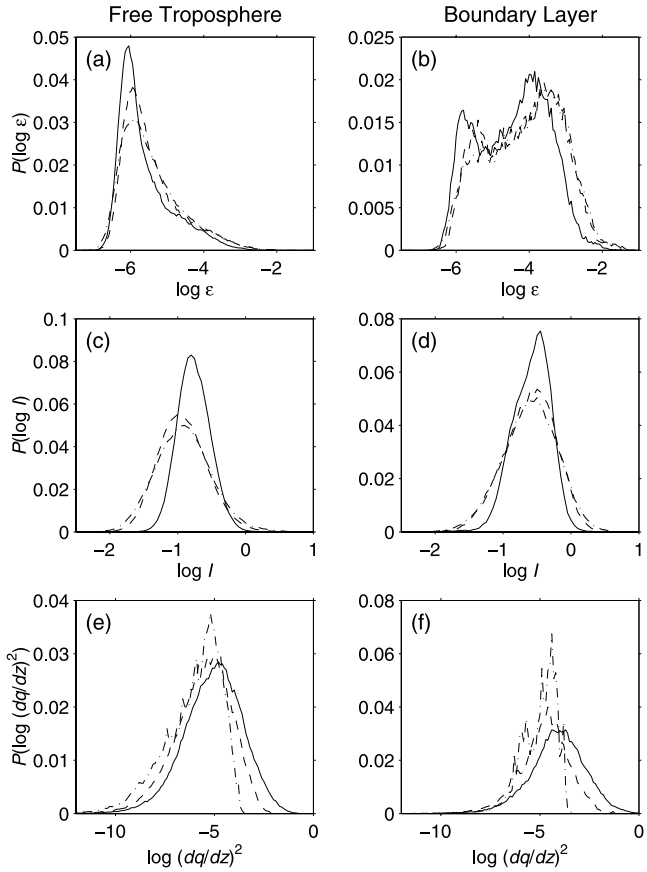

Figure 4. PDFs of log ϵ and log I for $\Delta t = 0.05$ s (solid), 0.25 s (dashed), and 0.5 s (dash-dotted). Also PDFs of log $(dq/dz)^2$ for $\Delta z = 10$ m (solid), 100 m (dashed), and 1000 m (dash-dotted). The left-hand column is for free tropospheric data and the right-hand column is for boundary layer data.

Table 1. Turbulence Parameters in the Free Troposphere

	ϵ, m^2 s^{-3}			I		
Δt, s	0.05	0.25	0.5	0.05	0.25	0.5
Mean	2.1×10^{-5}	4.5×10^{-5}	5.0×10^{-5}	0.21	0.18	0.21
Median	1.4×10^{-6}	2.2×10^{-6}	2.4×10^{-6}	0.17	0.11	0.12
Log-Mean	2.4×10^{-6}	3.6×10^{-6}	3.6×10^{-6}	0.17	0.12	0.12
Mode	8.9×10^{-7}	1.1×10^{-6}	1.3×10^{-6}	0.16	0.10	0.13

of specific humidity squared, $(dq/dz)^2 = [q(z + \Delta z) - q(z)]^2/(\Delta z)^2$; the Brunt–Väisälä frequency squared, $N^2 = (g/\theta)[\theta(z + \Delta z) - \theta(z)]/\Delta z$, where g is the gravitational acceleration, θ is the potential temperature, and $\bar{\theta}$ is the mean potential temperature; and the gradient Richardson number, $Ri = N^2/(dU/dz)^2$. Also, in order to assess the thermodynamic effects of humidity on stability, we computed N_v^2 and Ri_v where the differenced θ quantities are replaced by the virtual potential temperature θ_v for unsaturated conditions and by the equivalent potential temperature θ_e for saturated conditions.

[20] For statistics comparing ϵ and I to the gradient quantities, we interpolated ϵ and I to the same 1-m altitude grid used above in order to have exact coincidence.

4. Discussion of Results

4.1. Single-Parameter Probability Distribution Functions (PDFs)

[21] Figure 1 indicates the locations of the vertical profiles used in this paper. One sees that virtually all of the data were taken over water.

[22] Figure 2d gives the probability distribution function (PDF) of the number of data points used with respect to latitude. The PDFs in Figures 2a to 2c are divided into the free troposphere (solid lines) and the boundary layer (dashed lines). One can see that most of the data points were taken in the lower to midtroposphere. The relative humidity PDFs show a very dry mode for the free troposphere (but with a non-negligible tail at wet values) and a very wet mode for the boundary layer (not surprising since almost all the profiles were over water). The broad tail in the free tropospheric relative humidity PDF should give us a significant amount of data with which to examine the potential effect of humidity on CAT generation.

[23] Before we go on to discuss the statistics, let us look at an example profile. Figure 3 shows the vertical profiles of temperature (T), q, N^2, $(dU/dz)^2$, and log ϵ. For vertical gradient quantities $\Delta z = 100$ m was used. For the ϵ calculation $\Delta t = 0.05$ s was used. The vertical lines at log $\epsilon = -3$ indicate heights where $Ri \leq 1/4$, i.e., potentially unstable layers. There are a few interesting

Table 2. Turbulence Parameters in the Boundary Layer

	ϵ, m^2 s^{-3}			I		
Δt, s	0.05	0.25	0.5	0.05	0.25	0.5
Mean	2.6×10^{-4}	6.0×10^{-4}	7.0×10^{-4}	0.32	0.35	0.37
Median	4.5×10^{-5}	8.9×10^{-5}	9.6×10^{-5}	0.28	0.26	0.25
Log-Mean	3.5×10^{-5}	7.0×10^{-5}	7.6×10^{-5}	0.26	0.25	0.25
Mode	1.4×10^{-4}	2.5×10^{-4}	2.0×10^{-4}	0.35	0.32	0.32

Table 3. Vertical Gradient Parameters in the Free Troposphere

	$(dU/dz)^2$, s^{-2}			$(dq/dz)^2$, $g^2\ kg^{-2}\ m^{-2}$		
Δz, m	10	100	1000	10	100	1000
Mean	1.7×10^{-3}	2.3×10^{-4}	5.0×10^{-5}	5.5×10^{-4}	7.3×10^{-5}	1.1×10^{-5}
Median	4.8×10^{-4}	1.1×10^{-4}	3.0×10^{-5}	1.0×10^{-5}	3.6×10^{-6}	1.7×10^{-6}
Log-Mean	4.6×10^{-4}	9.3×10^{-5}	2.5×10^{-5}	8.3×10^{-6}	2.6×10^{-6}	8.5×10^{-7}
Mode	5.0×10^{-4}	1.3×10^{-4}	4.0×10^{-5}	1.6×10^{-5}	1.0×10^{-5}	6.3×10^{-6}

features to note. The high-humidity layer between ~2 km and ~2.7 km is bounded by layers of strong static stability (temperature inversions) and shear. This morphology suggests large-scale differential advection creating a distinct tracer layer. Whether the high static stability at its edges was also a result of the differential advection or the preexisting stability layers forced the differential advection is an open question. The high-humidity layer is also turbulent, with the $Ri < 1/4$ condition created by low or negative values of N^2. Perhaps as a result of the eddy mixing the layer appears well mixed, whereas there are sharp gradients in q at the stable edges. One wonders whether the high humidity contributed to the creation of a statically unstable environment within the layer. (The relative humidity in this layer was significantly below saturation, so it was probably not cloudy.) However, one can also see that the regions of potential instability as delineated by $Ri \leq 1/4$ does not always coincide with turbulent layers in other sections of this profile.

[24] The turbulent layer from ~3.8 km to ~4.2 km is also bounded by regions of high static stability and strong shear. Ozone (peaking at ~140 ppbv) and carbon monoxide measurements (not shown here) indicate that this layer came from the stratosphere, probably through a tropopause fold. Again, differential advection is indicated, but this time the layer is too dry to support the idea that humidity might have been the cause of the convective instability.

[25] Let us now move on to the statistical results. Figures 4a and 4b display the PDFs of log ϵ for the free troposphere and boundary layer. Values of Δt = 0.05 s (solid), 0.25 s (dashed), and 0.5 s (dash-dotted) were used. For a nominal airspeed of 150 m s^{-1}, these Δt values correspond to separations of r = 7.5, 37.5, and 75 m. Note the bimodal distribution for the boundary layer, clearly indicating a separation between calm and turbulent conditions. The demarcation seems to occur at $\epsilon \sim 10^{-5}$ m^2 s^{-3}. The free tropospheric PDFs have a single mode at very low values of ϵ and monotonically decreases with strength. This shows the very intermittent nature of turbulence outside of the boundary layer. The PDFs shift slightly to larger values with increasing Δt used in the calculation, which simply means that the assumption of local isotropy used in the formula does not always hold in the measured real world. Otherwise the calculated ϵ should not depend on Δt.

[26] The anisotropy can be more clearly observed in Figures 4c and 4d. In general, $I < 1$ (log $I < 0$), and there is a tendency for the PDFs to slide to lower values with increasing Δt, which is expected—the anisotropy should increase with scale. What is surprising is how few values are close to true isotropy. True, most of the data in the free troposphere were taken under calm conditions, but even for the boundary layer, where turbulent conditions were more prevalent, there were not many data points where $I \sim 1$.

[27] The mean, median, log-mean, and mode values from the above PDFs are collected in Tables 1 and 2. The boundary layer is clearly more turbulent and closer to isotropy (at the examined scales) than the free troposphere. The tendencies with respect to Δt apparent in the PDFs can also be discerned in these average values. Because the Δt = 0.05 s output come closest to the approximation of a locally isotropic inertial subrange, we will use only those results in the rest of the paper.

[28] Let us now examine the statistics of the vertical gradient quantities. Figures 4e and 4f show the PDFs of log $(dq/dz)^2$ for Δz = 10 m (solid), 100 m (dashed), and 1000 m (dash-dotted) in the free troposphere and boundary layer. Again, as expected, the gradients become weaker with increasing Δz. We also see that $(dq/dz)^2$ is close to a log-normal distribution, at least for Δz = 10 m. The various average values of the PDFs are given in Tables 3 and 4. The specific humidity gradients are stronger in the boundary layer than in the free troposphere at all scales. This implies that even though the mixing is more vigorous in the boundary layer, the background gradient generated by having the water vapor source at the surface and the sink at the top dominates the homogenizing effect of turbulence. The generally higher values of q in the boundary layer also contributes to this difference since the gradients were not computed as fractional changes in specific humidity.

[29] The PDFs of the vertical shear in horizontal winds are displayed in Figures 5a and 5b. Again, $(dU/dz)^2$ appears to be log-normally distributed, and the values decreasing

Table 4. Vertical Gradient Parameters in the Boundary Layer

	$(dU/dz)^2$, s^{-2}			$(dq/dz)^2$, $g^2\ kg^{-2}\ m^{-2}$		
Δz, m	10	100	1000	10	100	1000
Mean	1.7×10^{-2}	4.4×10^{-4}	6.2×10^{-5}	5.3×10^{-3}	3.3×10^{-4}	3.2×10^{-5}
Median	2.7×10^{-3}	1.7×10^{-4}	3.7×10^{-5}	8.6×10^{-5}	2.0×10^{-5}	1.4×10^{-5}
Log-Mean	2.4×10^{-3}	1.5×10^{-4}	3.2×10^{-5}	7.3×10^{-5}	1.5×10^{-5}	9.2×10^{-6}
Mode	2.0×10^{-3}	2.0×10^{-4}	1.0×10^{-4}	2.0×10^{-4}	2.5×10^{-5}	4.0×10^{-5}

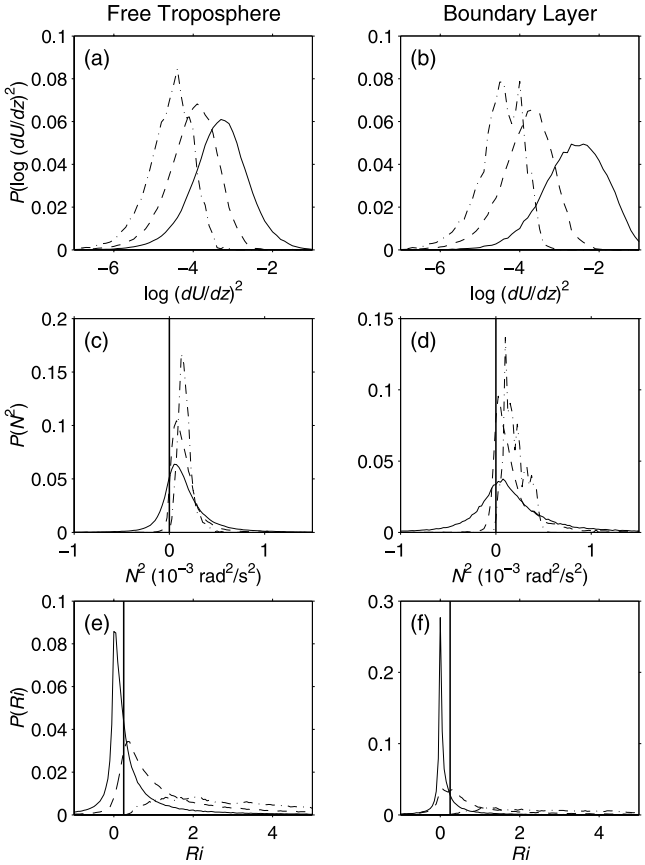

Figure 5. PDFs of log $(dU/dz)^2$, N^2, and Ri for $\Delta z = 10$ m (solid), 100 m (dashed), and 1000 m (dash-dotted). The left-hand column is for free tropospheric data and the right-hand column is for boundary layer data. The vertical lines in (c) and (d) mark $N^2 = 0$. The vertical lines in (e) and (f) mark the critical $Ri = 1/4$ level.

with increasing Δz. Average quantities are listed in Tables 3 and 4.

[30] The PDFs of N^2 shown in Figures 5c and 5d indicate a tendency to shift to lower values with increasing Δz. However, if one only looks at the mean values this would not be apparent (Tables 5 and 6). This tendency is most apparent in the mode values. Perhaps a more physically relevant parameter for turbulence is the percentage of data with $N^2 \leq 0$ values, which indicates a convectively unstable situation. Table 7 lists these values. Note the strong dependency of this parameter on Δz. We also see that the boundary layer is generally more convectively unstable than the free troposphere.

[31] We can combine the shear and static stability measures to get Ri. The PDFs are shown in Figures 5e and 5f. There is a strong dependence on Δz, which is clearly displayed in Tables 8 and 9. Again, the critical parameter is the percentage of data with $Ri \leq 1/4$ values, and these are tabulated in Table 10. Do these numbers imply that more than half of 10-m layers were potentially unstable? Not necessarily. As discussed earlier, the concept of "vertical profile" at 10-m may not be valid, and also the signals at these small scales may include a great deal of statistical noise. In terms of the use of these gradient quantities as a background against which turbulence might be generated, the $\Delta z = 100$ m values are probably most reasonable. The location of the modes of the Ri PDFs close to 1/4 for $\Delta z = 100$ m also supports this proposition, since convective adjustment of the atmosphere may tend to "pile up" Ri numbers near the critical value of 1/4 for scales within the typical outer scale of turbulence.

[32] We can compare the N^2 and Ri results with those of N_v^2 and Ri_v. The latter quantities include the thermodynamic effects of water vapor on static stability. The PDFs are plotted in Figure 6 and the average quantities listed in Tables 5 through 10. The effects are negligible in the free troposphere, but even in the boundary layer the effects are quite small, providing only slightly more potential instability in the atmosphere. We will go ahead and use N_v^2 and Ri_v instead of N^2 and Ri in the rest of the paper in order to include the effects of water vapor.

4.2. Parameter Dependencies

[33] In order to study the dependence of one parameter on another, we computed joint PDFs for pairs of variables. The $\Delta z = 100$ m quantities were used for the vertical gradient parameters, since we saw that this thickness was probably most reasonable to assume for the turbulence outer scale. As stated before, the $\Delta t = 0.05$ s results were used for ϵ and I. Plotting the full two-dimensional joint PDFs would take up much space in these pages, so we decided to simply graph the median values of one variable against the values of the other variable, which is a more compact representation and yet retains much of the essential information. An example of a median plot overlaid on a joint PDF contour plot is given in Figure 7.

[34] Figure 8a shows the dependency of the isotropy ratio I on ϵ. For $\epsilon > 10^{-6}$ m^2 s^{-3} I increased with ϵ, which is consistent with the usual assumption that fully developed turbulence is more isotropic than weak turbulence. The reversal of the trend for $\epsilon < 10^{-6}$ m^2 s^{-3} probably indicates that the velocity fluctuations were disappearing below the instrumental noise floor at these levels. (Presumably instrumental noise would be more isotropic than the atmospheric fluctuations.) Note that the trends were almost exactly the same for the free troposphere (solid

Table 5. Static Stability Parameters in the Free Troposphere

	N^2, rad^2 s^{-2}			N_v^2, rad^2 s^{-2}		
Δz, m	10	100	1000	10	100	1000
Mean	1.6×10^{-4}	1.6×10^{-4}	1.7×10^{-4}	1.5×10^{-4}	1.5×10^{-4}	1.6×10^{-4}
Median	1.1×10^{-4}	1.3×10^{-4}	1.5×10^{-4}	1.1×10^{-4}	1.2×10^{-4}	1.5×10^{-4}
Mode	5.0×10^{-5}	7.5×10^{-5}	1.3×10^{-4}	7.5×10^{-5}	7.5×10^{-5}	1.5×10^{-4}

Table 6. Static Stability Parameters in the Boundary Layer

	N^2, rad^2 s^{-2}			N_v^2, rad^2 s^2		
Δz, m	10	100	1000	10	100	1000
Mean	2.1×10^{-4}	2.1×10^{-4}	2.1×10^{-4}	1.9×10^{-4}	1.9×10^{-4}	1.9×10^{-4}
Median	1.1×10^{-4}	1.1×10^{-4}	1.8×10^{-4}	9.3×10^{-5}	9.3×10^{-5}	1.6×10^{-4}
Mode	7.5×10^{-5}	2.5×10^{-5}	1.0×10^{-4}	5.0×10^{-5}	2.5×10^{-5}	1.0×10^{-4}

line) and the boundary layer (dashed line), implying a universality to this dependency.

[35] Figure 8b shows that for $\epsilon > 10^{-6}$ m^2 s^{-3}, ϵ increased with shear. This trend seems to increase at the largest ϵ values. This dependency suggests that shear instability is a key controller of turbulence intensity, both in the free troposphere and the boundary layer.

[36] In contrast, we have Figure 9a, which suggests that static stability has a noticeable influence on turbulence intensity in the boundary layer but not in the free troposphere. Note the independence of N_v^2 and ϵ in the free troposphere, whereas in the boundary layer N_v^2 tends to decrease with ϵ. (The spike in free tropospheric data at the high ϵ end is due to too few data points for good statistics.) The percentage of data with $N_v^2 \leq 0$ vs. log ϵ is graphed in Figure 9c, showing again the importance of statically unstable conditions for turbulence production in the boundary layer.

[37] In an attempt to differentiate between the contributions of shear vs. convective instabilities to turbulence generation, we calculated the percentage of data with $Ri_v \leq 0$ and $0 < Ri_v$ 1/4. The former includes all convectively unstable situations, while the latter includes only (potentially) dynamically unstable conditions. The results are plotted in Figures 10a and 10b. In the free troposphere, the ratio of shear-produced turbulence to convectively produced turbulence increases from roughly 2:1 for weak turbulence ($\epsilon < 10^{-4}$ m^2 s^{-3}) to perhaps 3:1 for strong turbulence ($\epsilon > 10^{-4}$ m^2 s^{-3}). For the boundary layer, this ratio is close to 1:1 for weak turbulence and roughly 2:1 for strong turbulence.

[38] It is of interest to note that shear and static stability are not statistically independent. In fact, Figure 8f clearly shows that for a statically stable environment, shear and static stability are positively correlated. This dependency further sharpens the division between dynamically unstable and convectively unstable conditions.

[39] Finally we examine the relationship of the vertical gradient in specific humidity to the other variables. The motivation was to see if statistically we could discern the types of correlations we noted in Figure 3 between gradients in a tracer (specific humidity) and turbulence or static stability. From simple physical reasoning we might expect that strong tracer gradients would be correlated with statically stable layers and that weak gradients would be correlated with the smoothing effects of turbulent layers. (Strong humidity gradients can also cause differential radiative heating/cooling, which could indirectly affect the static stability.)

[40] Results exhibited in Figures 8c and 8e indicate that vertical humidity gradients are not strongly affected by turbulence. Figure 8d shows some positive correlation between shear and tracer gradient, which suggests differential advection as a key player in generating vertical tracer gradients. Static stability also increased with $(dq/dz)^2$ for strong humidity gradients (Figure 9b), which validates the idea that static stability impedes vertical mixing of tracer layers. In the boundary layer, the percentage of data with $N_v^2 \leq 0$ does seem to decrease with increasing $(dq/dz)^2$ in the mid-range of humidity gradient values (Figure 9d), and this is also reflected in the percentages of data with Ri_v below the critical thresholds (Figure 10d). A similar but weaker tendency can be observed in the free troposphere (Figures 9d and 10c). The weakness of the correlation may be the result of two offsetting factors: Ri_v is lowered by increased shear and becomes negative when N_v^2 goes negative, but while the former is associated with increased $(dq/dz)^2$ (Figure 8d), the latter condition is associated with decreased $(dq/dz)^2$.

5. Conclusions

[41] The data set used for this study is not necessarily representative of the global troposphere. Almost all the profiles were flown over the ocean, the latitudinal coverage was limited to between 15°N and 45°N, and the maximum height was less than 8 km. However, there were 122 vertical profiles used with a total of over 300 km in vertical airspace sampled. The 20-Hz resolution provided a wide range of spatial scales to examine. The PDFs calculated for the various quantities were reasonably well-behaved, and certain patterns and trends emerged that appeared to have physical significance.

[42] First, the PDFs of log ϵ had very different forms for the free troposphere and the boundary layer. For the former, the PDF was unimodal with the peak at $\sim 10^{-6}$ m^2 s^{-3} and a broad tail extending to higher values. For the latter,

Table 7. Percentage of Data With N^2 and N_v^2 Values ≤ 0

	N^2			N_v^2		
Δz, m	10	100	1000	10	100	1000
Free Troposphere	25	6.9	0.054	25	6.3	0.018
Boundary Layer	37	18	0.97	38	21	1.3

Table 8. Dynamic Stability Parameters in the Free Troposphere

	Ri			Ri_v		
Δz, m	10	100	1000	10	100	1000
Mean	2.5	9.4	75	2.3	9.2	76
Median	0.18	0.98	4.8	0.18	0.95	4.6
Mode	0.0	0.35	2.0	0.050	0.35	1.4

Table 9. Dynamic Stability Parameters in the Boundary Layer

	Ri			Ri_v		
Δz, m	10	100	1000	10	100	1000
Mean	5.9	7.9	110	6.3	6.3	92
Median	0.025	0.56	4.2	0.022	0.47	3.8
Mode	0.0	0.050	1.1	0.0	0.050	1.1

the PDF was bimodal with a similar "calm" peak and a higher "turbulent" peak at $\sim 10^{-4}$ m^2 s^{-3}. The implication is that the (marine) boundary layer is populated by distinct laminar and turbulent flow conditions and that the latter condition is more prevalent. Because our definition of the boundary layer included what some call the buffer layer (a region between the top of the well-mixed layer and the base of the capping inversion), the calm peak may be the result of the intermittently turbulent nature of the buffer layer. In the free troposphere, on the other hand, the background "basic" state is calm and turbulence occurs only intermittently.

[43] Second, the PDFs of the isotropy ratio I showed that anisotropy (horizontal velocity fluctuations greater than vertical velocity fluctuations) prevailed even down to the limit of spatial resolution ($\sim$8 m). This was true even for the boundary layer where turbulent conditions were common. However, the degree of isotropy did increase with decreasing scale as expected, and the boundary layer velocity fluctuations were more isotropic than the free tropospheric fluctuations.

[44] Third, we estimated that in the free troposphere, the ratio of shear-produced turbulence to convectively produced turbulence increased from roughly 2:1 for weak turbulence ($\epsilon < 10^{-4}$ m^2 s^{-3}) to perhaps 3:1 for strong turbulence ($\epsilon > 10^{-4}$ m^2 s^{-3}). For the boundary layer, this ratio was close to 1:1 for weak turbulence and roughly 2:1 for strong turbulence. We also noted a correlation between the strength of the vertical shear in horizontal winds and the turbulence intensity. In the free troposphere the turbulence intensity seemed to be independent of the degree of static stability, whereas in the boundary layer the turbulence intensity increased with a fall in static stability.

[45] Fourth, the thermodynamic effect of water vapor on static stability was negligible in the free troposphere. This effect was noticeable but still small in the boundary layer. We must note, however, that the flights on this mission tended to avoid areas of clouds because of certain objectives set by the chemistry program. Also, the season was late winter to early spring when the sea surface temperatures were low. We cannot rule out an influence of water vapor on the static stability of layers through differential radiative heating/cooling from these results—that type of study is outside the scope of this paper.

Table 10. Percentage of Data With *Ri* and Ri_v Values $\leq 1/4$

	Ri			Ri_v		
Δz, m	10	100	1000	10	100	1000
Free Troposphere	54	12	0.026	55	11	0.029
Boundary Layer	76	29	0.36	77	33	0.43

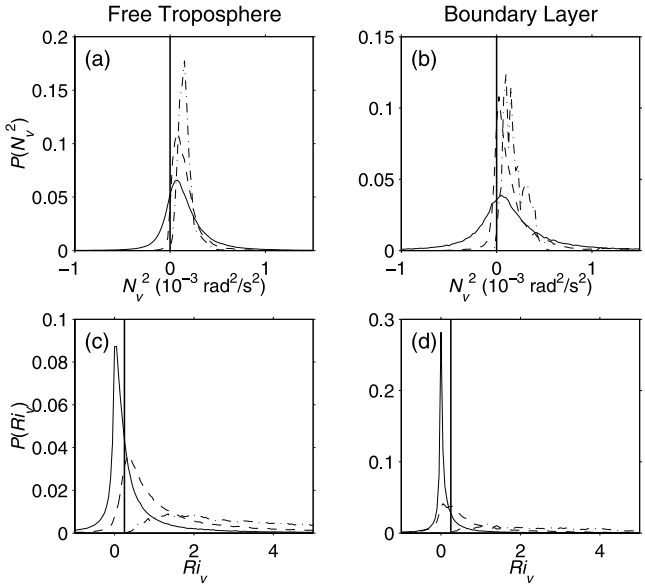

Figure 6. PDFs of N_v^2 and Ri_v for $\Delta z = 10$ m (solid), 100 m (dashed), and 1000 m (dash-dotted). The left-hand column is for free tropospheric data and the right-hand column is for boundary layer data. The vertical lines in (a) and (b) mark $N_v^2 = 0$. The vertical lines in (c) and (d) mark the critical $Ri_v = 1/4$ level.

[46] Finally, vertical humidity gradients did correlate statistically with static stability for strong humidity gradients, which supports the basic notion that stable layers impede vertical mixing of trace gases and aerosols. Vertical shear correlated with vertical humidity gradient, so it appears that the effect of differential advection creating

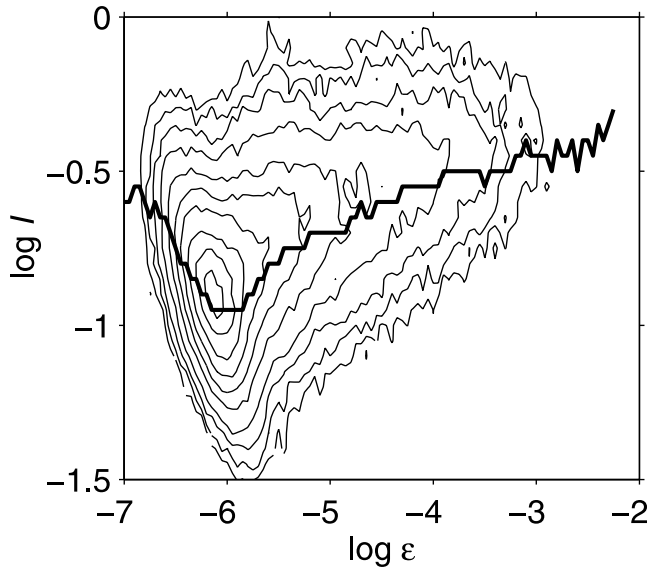

Figure 7. Contour plot of log I vs. log ϵ joint PDF for free tropospheric data. The PDF was normalized by the sum of the number of data points in all bins. The contour values are $10^{-3} \times$ [5 4 3 2 1.3 0.8 0.4 0.2 0.1 0.05]. The heavy line represents the median value of log I for the corresponding log ϵ bins.

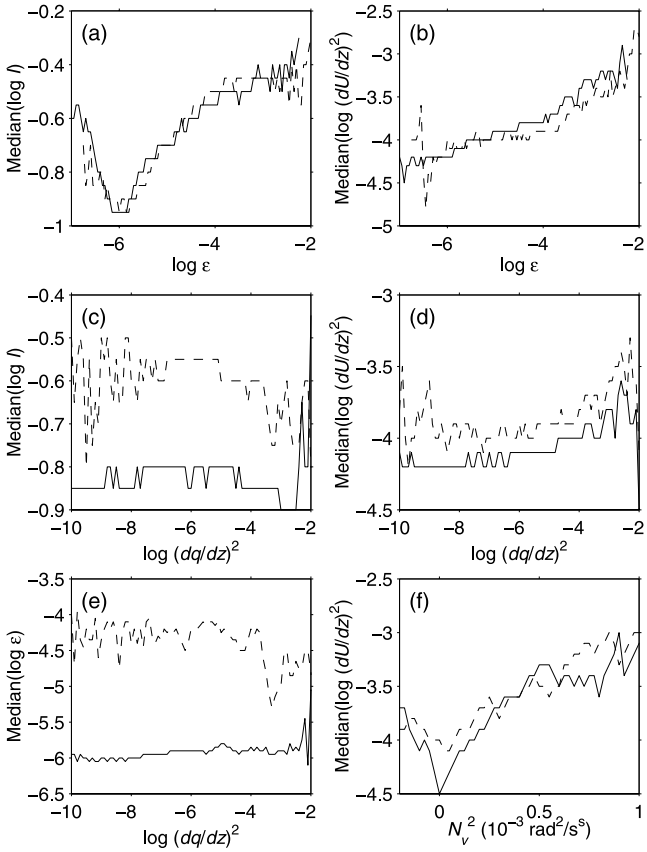

Figure 8. Plots of (a) the median of log I vs. log ϵ, (b) the median of log $(dU/dz)^2$ vs. log ϵx, (c) the median of log I vs. log $(dq/dz)^2$, (d) the median of log $(dU/dz)^2$ vs. log $(dq/dz)^2$, (e) the median of log ϵ vs. log $(dq/dz)^2$, and (f) the median of log $(dU/dz)^2$ vs. N_v^2. Solid lines denote free tropospheric data, and dashed lines denote boundary layer data.

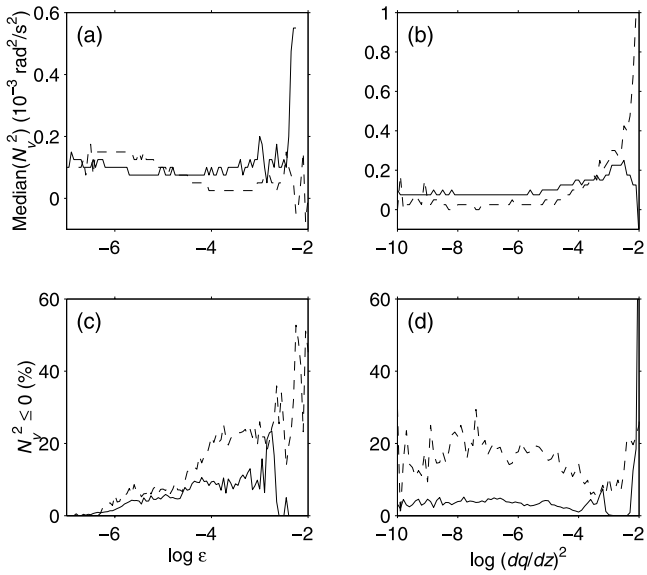

Figure 9. Plots of (a) the median of N_v^2 vs. log ϵ, (b) the median of N_v^2 vs. log $(dq/dz)^2$, (c) the percentage of data with $N_v^2 \leq 0$ vs. log ϵ, and (d) the percentage of data with $N_v^2 \leq 0$ vs. log $(dq/dz)^2$. Solid lines denote free tropospheric data, and dashed lines denote boundary layer data.

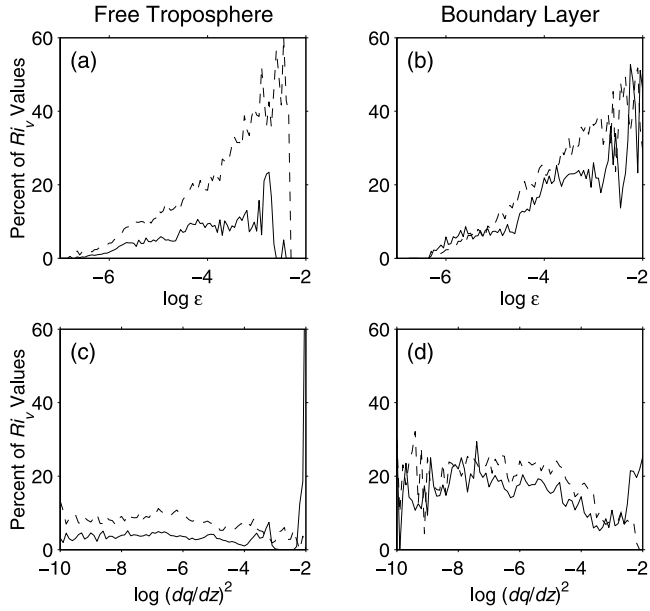

Figure 10. Percentage of data with (solid) $Ri_v \leq 0$ and (dashed) $0 < Ri_v$ 1/4. (a) and (b) are plotted against log ϵ, while (c) and (d) are plotted against log $(dq/dz)^2$. The free tropospheric cases are in the left-hand column and the boundary layer cases are in the right-hand column.

tracer gradients dominated the effect of differential advection destroying tracer gradients through KHI-induced turbulence on average.

[47] **Acknowledgments.** We would like to dedicate this paper to our dear friend and colleague (and coauthor of this paper), Reg Newell, who passed away on December 29, 2002. Reg was one of the prime movers behind NASA's Global Tropospheric Experiment, and his vision and enthusiasm will be sorely missed. The MIT work was funded by NASA grants NCC1-415 and NAG1-2306. We wish to thank Donald Bagwell for putting together the TAMMS data acquisition system and providing programming support.

References

Bacmeister, J. T., P. A. Newman, B. L. Gary, and K. R. Chan, An algorithm for forecasting mountain wave-related turbulence in the stratosphere, *Weather Forecasting*, *9*, 241–253, 1994.

Barrick, J. D. W., J. A. Ritter, C. E. Watson, M. W. Wynkoop, J. K. Quinn, and D. R. Norfolk, Calibration of NASA turbulent air motion measurement system, *NASA Tech. Pap., TP-3610*, 1996.

Charney, J. G., Geostrophic turbulence, *J. Atmos. Sci.*, *28*, 1087–1095, 1971.

Cho, J. Y. N., et al., Observations of convective and dynamical instabilities in tropopause folds and their contribution to stratosphere-troposphere exchange, *J. Geophys. Res.*, *104*, 21,549–21,568, 1999.

Cho, J. Y. N., R. E. Newell, E. V. Browell, W. B. Grant, C. F. Butler, and M. A. Fenn, Observation of pollution plume capping by a tropopause fold, *Geophys. Res. Lett.*, *28*, 3243–3246, 2001.

Considine, G. D., B. Anderson, J. Barrick, and D. H. Lenschow, Characterization of turbulent transport in the marine boundary layer during flight 7 of PEM-Tropics A, *J. Geophys. Res.*, *104*, 5855–5863, 1999.

Dalaudier, F., C. Sidi, M. Crochet, and J. Vernin, Direct evidence of "sheets" in the atmospheric temperature field, *J. Atmos. Sci.*, *51*, 237–248, 1994.

Ellrod, G. P., and D. I. Knapp, An objective clear-air turbulence forecasting technique: Verification and operational use, *Weather Forecasting*, *7*, 150–165, 1992.

Fuelberg, H. E., C. Kiley, J. R. Hannan, D. J. Westberg, M. A. Avery, and R. E. Newell, Meteorological conditions and transport pathways during the transport and chemical evolution over the Pacific (TRACE-P) experiment, *J. Geophys. Res.*, *108*(D20), 8782, doi:10.1029/2002JD003092, in press, 2003.

Haynes, P., and J. Anglade, The vertical-scale cascade in atmospheric tracers due to large-scale differential advection, *J. Atmos. Sci.*, *54*, 1121–1136, 1997.

Hobbs, P. V., Clean air slots amid atmospheric pollution, *Nature*, *415*, 861, 2002.

Hocking, W. K., S. Fukao, M. Yamamoto, T. Tsuda, and S. Kato, Viscosity waves and thermal-conduction waves as a cause of "specular" reflectors in radar studies of the atmosphere, *Radio Sci.*, *26*, 1281–1303, 1991.

Hooke, W. H., and R. M. Jones, Dissipative waves excited by gravity-wave encounters with the stably stratified planetary boundary layer, *J. Atmos. Sci.*, *43*, 2048–2060, 1986.

Jacob, D. J., J. Crawford, M. M. Kleb, V. S. Connors, R. J. Bendura, J. L. Raper, G. W. Sachse, J. Gille, L. Emmons, and J. C. Heald, Transport and chemical evolution over the Pacific (TRACE-P) mission: Design, execution, and first results, *J. Geophys. Res.*, *108*(D20), 8781, doi:10.1029/2002JD003276, in press, 2003.

McNeal, R. J., J. P. Mugler Jr., R. C. Harriss, and J. M. Hoell Jr., NASA Global Tropospheric Experiment, *Eos Trans. AGU*, *64*, 561–562, 1983.

Meischner, P., R. Baumann, H. Höller, and T. Jank, Eddy dissipation rates in thunderstorms estimated by Doppler radar in relation to aircraft in situ measurements, *J. Atmos. Oceanic Technol.*, *18*, 1609–1627, 2001.

Monin, A. S., and A. M. Yaglom, *Statistical Fluid Mechanics: Mechanics of Turbulence*, vol. 2, 874 pp., MIT Press, Cambridge, Mass., 1975.

Muschinski, A., and C. Wode, First in-situ evidence for co-existing submeter temperature and humidity sheets in the lower free troposphere, *J. Atmos. Sci.*, *55*, 2893–2906, 1998.

Newell, R. E., V. Thouret, J. Y. N. Cho, P. Stoller, A. Marenco, and H. G. Smit, Ubiquity of quasi-horizontal layers in the troposphere, *Nature*, *398*, 316–319, 1999.

Paluch, I. R., and D. G. Baumgartner, Entrainment and fine-scale mixing in a continental convective cloud, *J. Atmos. Sci.*, *46*, 261–278, 1989.

Panofsky, H. A., and J. A. Dutton, *Atmospheric Turbulence*, 397 pp., John Wiley, Hoboken, N. J., 1984.

Russell, L. M., D. H. Lenschow, K. K. Laursen, P. B. Krummel, S. T. Siems, A. R. Bandy, D. C. Thornton, and T. S. Bates, Bidirectional mixing in an ACE 1 marine boundary layer overlain by a second turbulent layer, *J. Geophys. Res.*, *103*, 16,411–16,432, 1998.

Smyth, W. D., and J. N. Moum, Anisotropy of turbulence in stably stratified mixing layers, *Phys. Fluids*, *12*, 1343–1362, 2000.

Swap, R. J., and P. D. Tyson, Stable discontinuities as determinants of the vertical distribution of aerosols and trace gases in the atmosphere, *S. Afr. J. Sci.*, *95*, 63–71, 1999.

Weinstock, J., On the theory of turbulence in the buoyancy subrange of stably stratified flows, *J. Atmos. Sci.*, *35*, 634–649, 1978.

Woods, J. D., On Richardson's number as a criterion for laminar-turbulent-laminar transition in the ocean and atmosphere, *Radio Sci.*, *4*, 1289–1298, 1969.

B. E. Anderson, J. D. W. Barrick, and K. L. Thornhill, NASA Langley Research Center, Mail Stop 483,21 Langley Boulevard, Hampton, VA 23681-2199, USA. (b.e.anderson@larc.nasa.gov; j.d.barrick@larc.nasa.gov; k.l.thornhill@larc.nasa.gov)

J. Y. N. Cho, Lincoln Laboratory, Massachusetts Institute of Technology, 244 Wood Street, Lexington, MA 02420-9185, USA. (jync@mit.edu)

R. E. Newell, Department of Earth, Atmospheric, and Planetary Sciences, Massachusetts Institute of Technntiology, 77 Massachusetts Ave., MS 54-1824, Cambridge, MA 02139-4307, USA. (renewell@mit.edu)